Sensitivity analysis for elastic full-waveform inversion in VTI media

Nishant Kamath & Ilya Tsvankin
Center for Wave Phenomena, Colorado School of Mines

ABSTRACT

Multiparameter full-waveform inversion (FWI) is generally nonunique, and the results are strongly influenced by the geometry of the experiment and the type of recorded data. Studying the sensitivity of different subsets of data to the model parameters may help in choosing an optimal acquisition design, inversion workflow, and parameterization. Here, we derive the Fréchet kernel for FWI of multicomponent data from a 2D VTI (tranversely isotropic with a vertical symmetry axis) medium. The kernel is obtained by linearizing the elastic wave equation using the Born approximation and employing the asymptotic Green's function. The amplitude of the kernel ('radiation pattern') yields the angle-dependent energy scattered by a perturbation in a certain model parameter. The perturbations are described in terms of the P- and S-wave vertical velocities and the P-wave normal-moveout and horizontal velocities. The background medium is assumed to be homogeneous and isotropic, which allows us to obtain simple expressions for the radiation patterns corresonding to all four velocities. These patterns help explain the FWI results for multicomponent transmission data generated for Gaussian anomalies in the Thomsen parameters inserted into a homogeneous VTI medium.

1 INTRODUCTION

Full-waveform inversion (FWI) of seismic data is often performed under the assumption of an acoustic and isotropic earth model. In that case, the wavefield is described by a single spatially varying parameter – the P-wave velocity. Taking elasticity and/or anisotropy into account introduces additional parameter fields, and the outcome of the inversion strongly depends on the choice of model parameterization.

The sensitivity of FWI to a chosen set of parameters has been studied for acoustic VTI media. The P-waves kinematics in VTI models can be described by the vertical velocity V_{P0}, the normal-moveout velocity $V_{\rm nmo}$ ($V_{\rm nmo} = V_{P0}\sqrt{1+2\delta}$), and the horizontal velocity $V_{\rm hor}$ ($V_{\rm hor} = V_{P0}\sqrt{1+2\epsilon}$). Employing the singular value decomposition (SVD) of the Fréchet derivative matrix ('sensitivity matrix'), Plessix and Cao (2011) evaluate the sensitivity of the objective function to the VTI parameters. Gholami et al. (2011) carry out inversion either for a single velocity (V_{P0}, $V_{\rm nmo}$, or $V_{\rm hor}$) while keeping the other two at the actual values or for two velocities (V_{P0} and $V_{\rm hor}$) simultaneously. They conclude that the single-parameter inversion provides a good estimate of the unknown velocity, while the multiparameter inversion suffers from trade-offs.

The Fréchet kernel of FWI relates a perturbation in the wavefield to perturbations in the model parameters. Gholami et al. (2013) use finite differences to compute the Fréchet kernel for a point diffractor embedded in a homogeneous acoustic VTI space. The amplitude of the kernel varies with the angle between the incident wave and the symmetry axis at the diffractor. This variation, called the "radiation pattern," helps evaluate the sensitivity of the inversion to model parameters. An analytic description of the radiation patterns associated with a VTI perturbation in a homogeneous isotropic medium is developed by Alkhalifah and Plessix (2013).

In a previous paper (Kamath and Tsvankin, 2014; hereafter referred to as Paper I), we perform FWI of multicomponent transmission data computed for Gaussian anomalies in the Thomsen parameters embedded in homogeneous elastic VTI models. The gradient of the objective function is obtained with the adjoint-state method. The medium is described by the P-wave vertical velocity V_{P0}, NMO velocity $V_{\rm nmo}$, horizontal velocity $V_{\rm hor}$, and the S-wave vertical velocity V_{S0}. Experiments performed for horizontal and vertical arrays of sources and receivers show strong dependence of the inversion results on the acquisition geometry.

Here, we perform sensitivity analysis of FWI for 2D VTI media parameterized by the velocities V_{P0}, V_{S0}, $V_{\rm nmo}$, and $V_{\rm hor}$. First, we derive the Fréchet kernel for elastic FWI using the Born and WKBJ approximations and an asymptotic representation of the Green's function. Then the kernel is used to obtain the radiation patterns for the relevant stiffness coefficients. Assuming a homogeneous isotropic background makes it possible to derive simple radiation patterns for the four velocities. Finally, the radiation patterns for the P- and S-wavefields are employed to explain the results of FWI for transmission data in Paper I.

2 METHODOLOGY

We consider an elastic, homogeneous, isotropic background medium with spatially varying perturbations in the stiffness coefficients. It should be emphasized that the perturbed stiffnesses correspond to an arbitrarily anisotropic, elastic medium. Assuming the background to be isotropic and homogeneous allows us to obtain relatively simple expressions for the radiation patterns.

Following Calvet et al. (2006) and Alkhalifah and Plessix (2013), we represent the elastic wave equation in the Born approximation for a perturbation δc_{ijkl} in the stiffness tensor:

$$\rho \frac{\partial^2 \delta u_i}{\partial t^2} - \frac{\partial}{\partial x_j}\left(c_{ijkl}\,\frac{\partial \delta u_k}{\partial x_l}\right) = \frac{\partial}{\partial x_j}\left(\delta c_{ijkl}\,\frac{\partial u_k}{\partial x_l}\right)\,, \tag{1}$$

where $\delta\mathbf{u}$ is the perturbation in the wavefield caused by the perturbation δc_{ijkl} in the stiffness tensor. The solution of equation 1 can be expressed in terms of the Green's functions G_{mk} and G_{ni} (Appendix A):

$$\delta u_n(\mathbf{x}_r,\omega) = -\int\limits_{V(\mathbf{x}')} f_m(\mathbf{x}_s,\omega)\,\delta c_{ijkl}(\mathbf{x}') \times \frac{\partial G_{mk}(\mathbf{x}_s,\mathbf{x}',\omega)}{\partial x'_l}\,\frac{\partial G_{ni}(\mathbf{x}_r,\mathbf{x}',\omega)}{\partial x'_j}\,dV(\mathbf{x}')\,, \tag{2}$$

where $\mathbf{x}_s$ and $\mathbf{x}_r$ are the locations of the source and receiver, respectively, $\mathbf{f}$ is the source function, and $V(x')$ is the volume that includes all scatterers. The Green's functions are then replaced by their asymptotic representation (Vavryčuk, 2007). Taking the spatial derivative of just the exponent of $\mathbf{G}$ (i.e., of its rapidly varying part, according to the WKBJ approximation) yields (equation A16):

$$\delta u_n(\mathbf{x}_r,\omega) = \int\limits_{V(\mathbf{x}')} f_m(\mathbf{x}_s,\omega)\,\mathcal{A}(\omega)\,p_l^s\,p_j^r\,g_k^s\,g_i^r\,\delta c_{ijkl}\,dV(\mathbf{x}')\,. \tag{3}$$

The superscripts s and r denote the incident and scattered wavefields, respectively, $\mathcal{A}(\omega)$ is a function of frequency and the background velocities of the incident and scattered wavefields, and $\mathbf{p}$ and $\mathbf{g}$ are the unit slowness and polarization vectors, respectively. The radiation pattern is the amplitude of the kernel that varies with the incident and scattering angles. For a model parameterized in terms of the stiffnesses, the radiation pattern derived from equation 3 is (equation A18):

$$\Omega = p_l^s\,p_j^r\,g_k^s\,g_i^r\,. \tag{4}$$

Equation 4 is valid for a perturbation δc_{ijkl} corresponding to an elastic, arbitrarily anisotropic scatterer in 3D. In this study, however, we consider a 2D elastic VTI medium, so the indices i, j, k, and l in equations $2-4$ take values of 1 and 3. The chain rule can then be used to obtain the pattern Ω for a VTI medium described in terms of the velocities V_{P0}, V_{S0}, $V_{\rm nmo}$, and $V_{\rm hor}$.

The normalized scattering coefficients for the P- and SV-wavefields are given by equations A23−A26 and A27− A30, respectively. In the case of the transmitted wavefield, the incidence and scattering angles coincide. Substituting equations A31 − A38 into equations A23 − A30, we obtain the radiation patterns (normalized by $2\rho\,V_{P0}$) for the scattered P-wavefield:

$$\Omega^P(V_{P0}) = 2\cos^2\theta\,, \tag{5}$$

$$\Omega^P(V_{S0}) = 0\,, \tag{6}$$

$$\Omega^P(V_{\rm nmo}) = \frac{1}{2}\sin^2 2\theta\,, \tag{7}$$

$$\Omega^P(V_{\rm hor}) = 2\sin^4\theta\,, \tag{8}$$

where θ is the incidence angle. The patterns for the scattered S-wavefield (also normalized by $2\rho\,V_{P0}$) are:

$$\Omega^S(V_{P0}) = 0\,, \tag{9}$$

$$\Omega^S(V_{S0}) = -2\frac{V_{S0}}{V_{P0}}\,, \tag{10}$$

$$\Omega^S(V_{\rm nmo}) = \frac{1}{2}\sin^2 2\theta\,, \tag{11}$$

$$\Omega^S(V_{\rm hor}) = \frac{1}{2}\sin^2 2\theta\,, \tag{12}$$

The absolute values of radiation patterns in Figure 1 show how perturbations in the velocities V_{P0}, $V_{\rm nmo}$, and $V_{\rm hor}$ scatter P-wave energy for different incidence angles. In our approximation, a perturbation in V_{S0} does not influence the scattered P-wavefield. As expected, the intensity of the wavefield scattered by a perturbation in V_{P0} reaches its maximum for propagation along the symmetry axis and goes to zero in the isotropy plane (Figure 1(a)). In contrast, a perturbation in $V_{\rm hor}$ produces the largest scattering in the isotropy plane, with a rapid decay toward the symmetry axis (Figure 1(c)). The maximum energy scattered by a perturbation in $V_{\rm nmo}$ is four times smaller than that for V_{P0} and corresponds to an angle of 45° with the symmetry axis (Figure 1(b)).

A perturbation in the velocity V_{S0} scatters the SV-wavefield uniformly for the entire range of incidence angles (Figure 2(a)), which is likely due to the fact that V_{S0} also represents the horizontal SV-wave velocity. The radiation patterns of $V_{\rm nmo}$ and $V_{\rm hor}$ (Figure 2(b) and 2(c), respectively) for SV-waves are similar to that of $V_{\rm nmo}$ for the P-wave (Figure 1(b)). The SV-wave is primarily influenced by V_{S0} and the parameter $\sigma = (V_{P0}/V_{S0})^2(\epsilon-\delta) = (V_{\rm hor}^2 - V_{\rm nmo}^2)/2V_{S0}^2$ (Tsvankin, 2012). Therefore, for a model described in terms of V_{P0}, V_{S0}, $V_{\rm nmo}$, and $V_{\rm hor}$, the SV-wavefield does not explicitly depend on the velocity V_{P0}. This explains why a perturbation in V_{P0} does not scatter SV-waves (equation 9).

3 ANALYSIS OF FWI OF TRANSMISSION DATA

Next, we employ the analytic results obtained above to explain the FWI results for transmission data from Paper I. The models include Gaussian anomalies in the parameters V_{P0}, V_{S0}, and ϵ embedded in a homogeneous VTI background. Although the

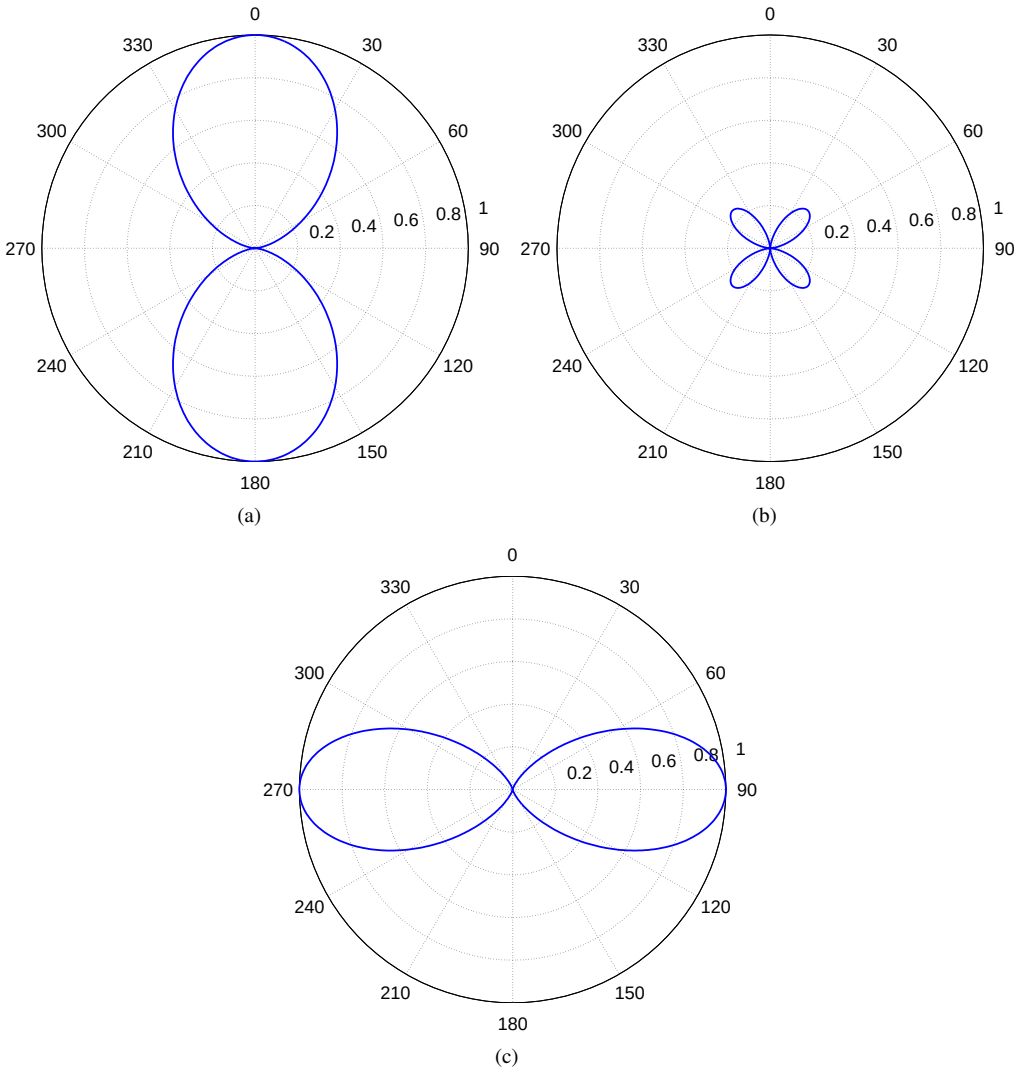

Figure 1. Radiation patterns of the velocities (a) V_{P0}, (b) $V_{\rm nmo}$, and (c) $V_{\rm hor}$ computed from equations 5, 7, and 8 (respectively) for the P-wavefield. The perturbations are inserted into an isotropic homogeneous background.

patterns in Figures 1 and 2 are derived for a purely isotropic background medium, we expect them to remain qualitatively valid when the background is moderately anisotropic.

The first test is performed for an anomaly in ϵ, which results in the corresponding perturbation in $V_{\rm hor}$. A vertical array of sources generates the P- and S-wavefields, and a vertical array of receivers on the other side of the anomaly records the data. For this source-receiver geometry, the aperture is about 51° on both sides of the isotropy plane. The amplitude of the scattered energy reduces by 50% at an angle of about $\pm 33^\circ$ from the horizontal (Figure 1(c)).

We run 50 iterations of FWI starting with the homogeneous background VTI model. As demonstrated in Paper I, there is negligible difference between the inverted and starting values of V_{P0} (Figure 4(a)), V_{S0} (Figure 4(b)), and $V_{\rm nmo}$. The algorithm updates only $V_{\rm hor}$, which helps accurately recover the anomaly in ϵ (Figure 4(c)) because V_{P0} remains unchanged. The estimated parameter δ, which depends on the ratio $V_{\rm nmo}/V_{P0}$, stays equal to the background value (Figure 4(d)).

These inversion results are well explained by the radiation patterns in Figure 1. For the aperture in the test, the radiation pattern of $V_{\rm hor}$ is decoupled from those of V_{P0}, V_{S0}, and $V_{\rm nmo}$. Hence, FWI updates only the horizontal velocity, which results in an appropriate change in the coefficient ϵ and an accurate inverted model.

Another model from Paper I includes an anomaly in V_{P0} with the same source-receiver configuration. Whereas the algorithm again updates $V_{\rm hor}$, it cannot significantly change V_{P0} and $V_{\rm nmo}$ because the aperture is insufficient to record most energy scattered by the anomalies in those velocities. Consequently, instead of the anomaly in V_{P0}, FWI generates a false

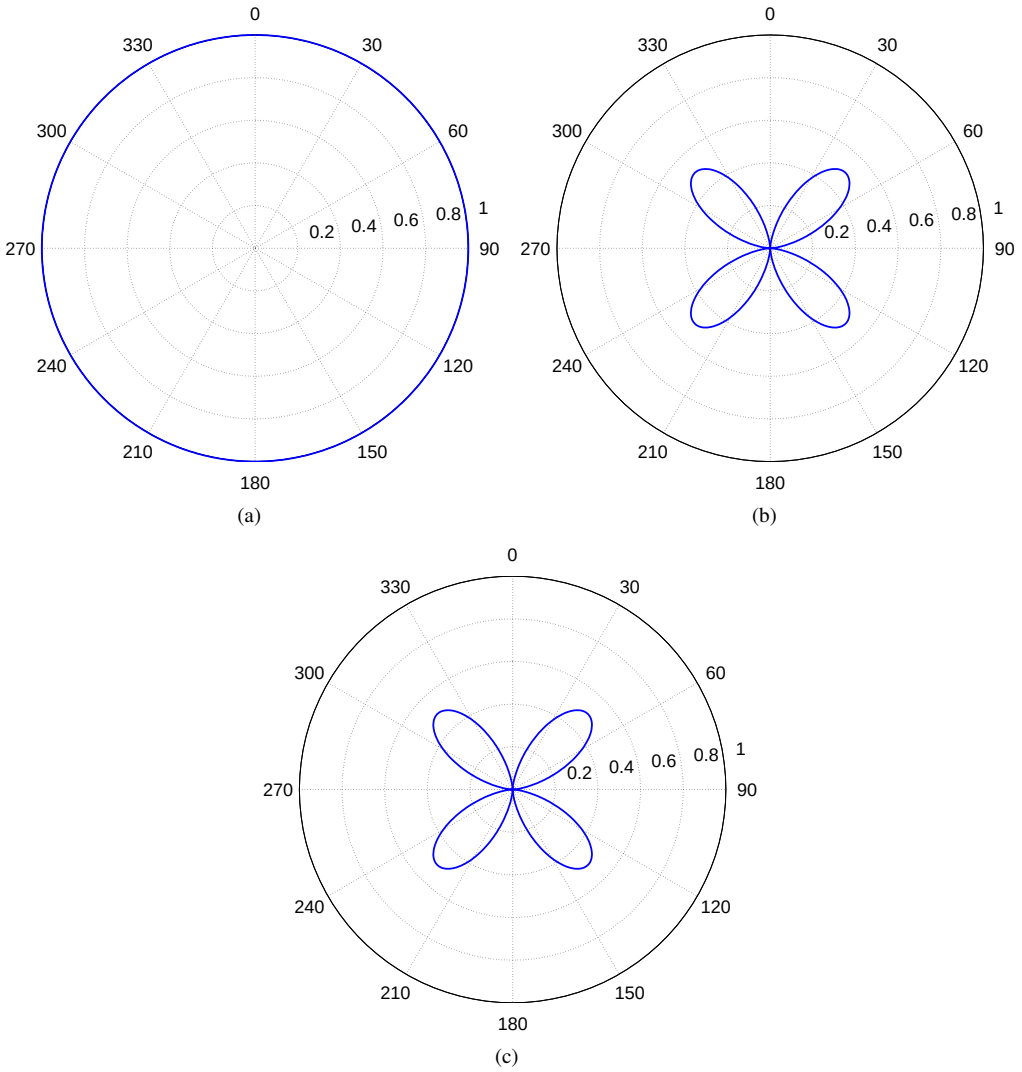

Figure 2. Radiation patterns of the velocities (a) V_{S0}, (b) $V_{\rm nmo}$, and (c) $V_{\rm hor}$ computed from equations 10, 11, and 12 (respectively) for the S-wavefield. The perturbations are inserted into an isotropic homogeneous background; the ratio $V_{S0}/V_{P0} = 0.5$.

anomaly in ϵ. As in the previous test, the algorithm correctly keeps the coefficient δ at the background value.

When the source-receiver configuration for the same model is rotated by 90° (Figure 5), the inversion algorithm predominantly updates V_{P0} (Figure 6(a)). Because the receivers do not record most of the energy scattered by the anomalies in $V_{\rm nmo}$ and $V_{\rm hor}$, the algorithm does not update these parameters. Hence, although the anomaly in V_{P0} is recovered, the parameters ϵ and δ, which depend on $V_{\rm hor}$ and $V_{\rm nmo}$, are distorted (Figures 6(c) and 6(d), respectively).

Whereas an anomaly in the velocity V_{S0} does not influence the P-wavefield, it scatters the S-wavefield equally in all directions (Figure 2(a)). As a result, the FWI algorithm operating with SV data can recover the anomaly in V_{S0} irrespective of the source-receiver configuration.

4 CONCLUSIONS

We presented a general approach for evaluating the sensitivity of elastic anisotropic FWI to model parameterization. A point diffractor corresponding to a perturbation in the stiffness coefficients was inserted into a homogeneous isotropic background medium. By employing the Born and WKBJ approximations along with an asymptotic representation of the Green's functions, we obtained an analytic expression for the Fréchet kernel of FWI.

For VTI media, the amplitude of the kernel ("radiation pattern") was expressed in terms of the P- and S-wave vertical velocities (V_{P0} and V_{S0}), and the P-wave NMO and horizontal velocities ($V_{\rm nmo}$ and $V_{\rm hor}$). Assuming an isotropic homogeneous background yields simple expressions for the radiation patterns of all four velocities. This methodology can be easily

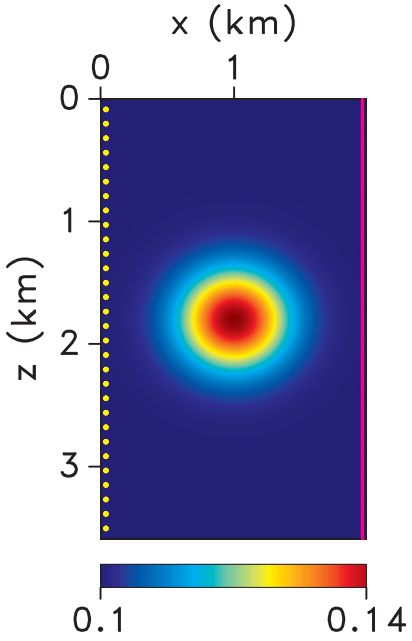

Figure 3. VTI model with a Gaussian anomaly (standard deviation $\sigma = 300\,\mathrm{m}$) in the anisotropy parameter ϵ (after Paper I). The background and maximum values of ϵ are 0.1 and 0.142, respectively. The other Thomsen parameters are spatially invariant: $V_{P0} = 3000\,\mathrm{m/s}$, $V_{S0} = 1500\,\mathrm{m/s}$, and $\delta = -0.05$. The dots on the left mark the source locations and the vertical line on the right represents an array of receivers placed at each grid point (6.6 m apart).

adapted to obtain radiation patterns for other model parameterizations.

The scattered P-wavefield in our approximation is insensitive to the velocity V_{S0}, whereas the radiation patterns of V_{P0} and V_{hor} are decoupled. An anomaly in V_{P0} scatters most of the P-wave energy in the vicinity ($\pm 45^\circ$) of the symmetry axis, so stable estimation of V_{P0} requires good wavefield sampling in that range of angles. In contrast, a perturbation in V_{hor} produces the largest P-wave scattering near the isotropy plane, which is favorable for crosshole geometry.

In our parameterization, the SV-wavefield is not scattered by the velocity V_{P0}. A perturbation in the velocity V_{S0} scatters the SV-wave energy uniformly in all directions, so elastic FWI can potentially recover V_{S0} for any aperture of the experiment.

An anomaly in the velocity V_{nmo} predominantly scatters both the P- and SV-wavefields near an angle of 45°, and the scattering amplitude is smaller than that of the other parameters. Hence, transmitted P- and SV-waves do not provide tight constraints on V_{nmo}. A better estimate of V_{nmo} may be obtained from reflected waves.

Our results indicate that if the background model is known and the receivers record energy propagating in the vicinity of the symmetry axis, FWI of multicomponent transmission data should be able to resolve the parameters V_{P0} and V_{S0}. In the case of crosshole geometry, it should be possible to estimate V_{hor} and V_{S0}.

This study was limited to analysis of the amplitude of the Fréchet kernel. By taking the phase of the kernel into account, our approach could be extended to FWI of reflection data.

5 ACKNOWLEDGMENTS

We are grateful to the members of the A(nisotropy) team at CWP, Tariq Alkhalifah (KAUST), and Andreas Rüger (Landmark Graphics) for fruitful discussions. This work was supported by the Consortium Project on Seismic Inverse Methods for Complex Structures at CWP and by the CIMMM Project of the Unconventional Natural Gas Institute at CSM. The reproducible numeric examples in this paper are generated with the Madagascar open-source software package freely available from http://www.ahay.org.

REFERENCES

Aki, K., and P. G. Richards, 2002, Quantitative seismology, 2nd ed.: University Science Books.

Alkhalifah, T., and R.-E. Plessix, 2013, A recipe for practical full waveform inversion in anisotropic media: An analytical parameter resolution study. Submitted.

Calvet, M., S. Chevrot, and A. Souriau, 2006, P-wave propagation in transversely isotropic media: I. finite-frequency theory: Physics of the Earth and Planetary Interiors, **156**, 12–20.

Gholami, Y., R. Brossier, S. Operto, V. Prieux, A. Ribodetti, and J. Virieux, 2011, Two-dimensional acoustic anisotropic (VTI) full waveform inversion: The Valhall case study: SEG Technical Program Expanded Abstracts, **30**, 2543–2548.

Gholami, Y., R. Brossier, S. Operto, A. Ribodetti, and J. Virieux, 2013, Which parameterization is suitable for

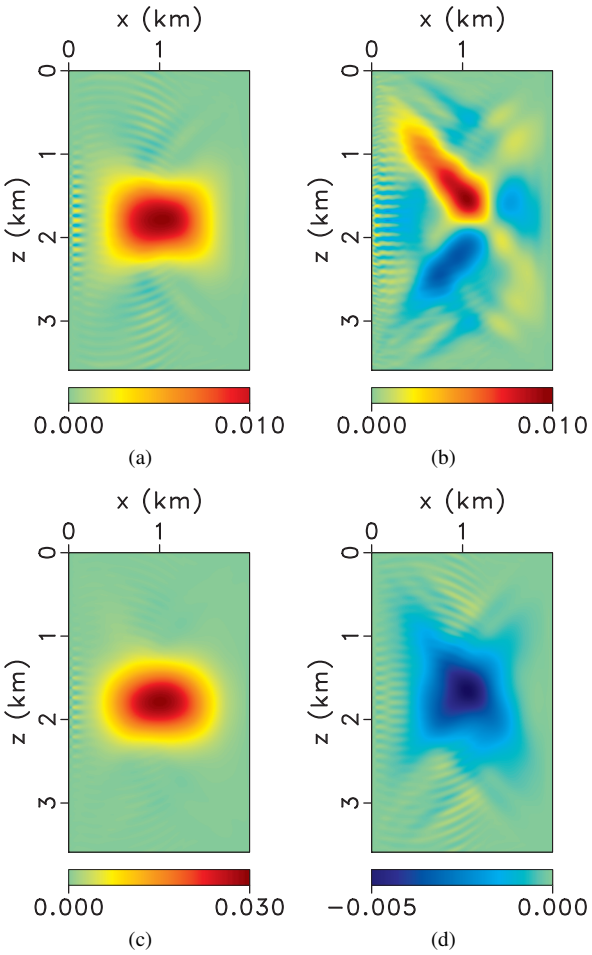

Figure 4. Difference between the inverted parameters (a) V_{P0}, (b) V_{S0}, (c) ϵ, and (d) δ and their initial values for the model from Figure 3 (after Paper I). The velocities have units of km/s.

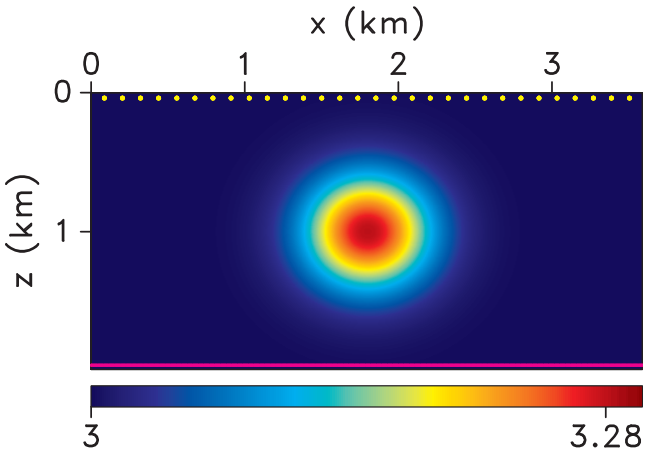

Figure 5. VTI model with a Gaussian anomaly in V_{P0} (after Paper I). The source and receiver arrays are horizontal.

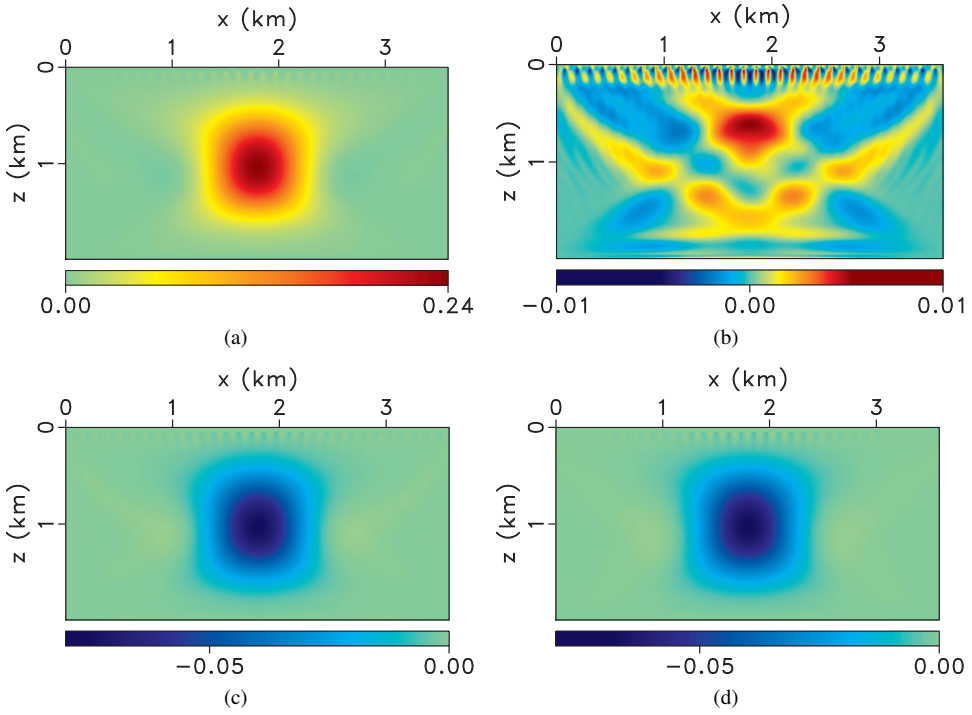

Figure 6. Difference between the inverted parameters (a) V_{P0}, (b) V_{S0}, (c) ϵ, and (d) δ and their initial values for the model from Figure 5 (after Paper I).

acoustic vertical transverse isotropic full waveform inversion? Part 1: Sensitivity and trade-off analysis: Geophysics, **78**, R81–R105.

Kamath, N., and I. Tsvankin, 2014, Elastic full-waveform inversion of transmission data in 2D VTI media: CWP Report, **783**.

Plessix, R., and Q. Cao, 2011, A parametrization study for surface seismic full waveform inversion in an acoustic vertical transversely isotropic medium: Geophysical Journal International, **185**, 539–556.

Tsvankin, I., 2012, Seismic signatures and analysis of reflection data in anisotropic media, 3rd ed.: Society of Exploration Geophysicists.

Vavryčuk, V., 2007, Asymptotic Green's function in homogeneous anisotropic viscoelastic media: Proceedings of the Royal Society A: Mathematical, Physical and Engineering Science, **463**, 2689–2707.

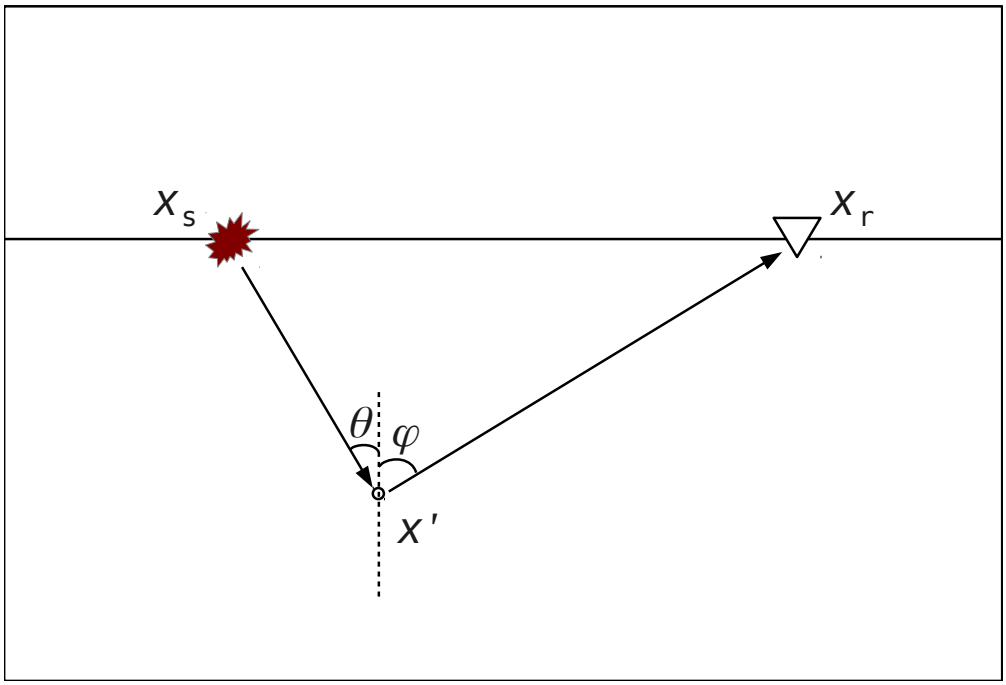

Figure A1. Geometry of the scattering experiment. The source is located at $\mathbf{x}_s$, the scatterer at $\mathbf{x}'$, and the receiver at $\mathbf{x}_r$.

APPENDIX A: SENSITIVITY PATTERNS FOR ELASTIC FWI IN VTI MEDIA

The radiation pattern is obtained by expressing the scattered wavefield in the Born approximation using the asymptotic Green's function. The wave equation for heterogeneous anisotropic media has the form:

$$\rho \frac{\partial^2 u_i}{\partial t^2} - \frac{\partial}{\partial x_j}\left(c_{ijkl}\frac{\partial u_k}{\partial x_l}\right) = f_i \ , \tag{A1}$$

where ρ is the density, c_{ijkl} are components of the stiffness tensor, and $\mathbf{f}$ is the body force per unit volume. All indices change from 1 to 3 and summation over repeated indices is implied. The displacement wavefield is subject to the initial conditions,

$$\mathbf{u}(\mathbf{x},0) = 0, \quad \frac{\partial \mathbf{u}(\mathbf{x},0)}{\partial t} = 0, \tag{A2}$$

and the radiation boundary condition,

$$\mathbf{u}(\mathbf{x},t)|_{\mathbf{x}\to\infty} \to 0. \tag{A3}$$

Suppose the wavefield produced by a source at $\mathbf{x}_s$ is scattered at $\mathbf{x}'$ and recorded by a receiver at $\mathbf{x}_r$. The background is taken to be homogeneous and isotropic, but the stiffness coefficients perturbed at $\mathbf{x}'$ correspond to those for the in-plane polarized waves in 2D VTI media (i.e., C_{11}, C_{13}, C_{33}, and C_{55}). A perturbation in the stiffness coefficient c_{ijkl} at the scatterer $\mathbf{x}'$ (Figure A1) results in a perturbation δu_i in the wavefield. We replace the wavefield u_i in equation A1 by $u_i = u_i^b + \delta u_i$ and the stiffnesses c_{ijkl} by $c_{ijkl} = c_{ijkl}^b + \delta c_{ijkl}$, where the superscript b refers to the background. Retaining only the terms linear in the perturbations in equation A1 leads to the Born approximation:

$$\rho \frac{\partial^2 \delta u_i}{\partial t^2} - \frac{\partial}{\partial x_j}\left(\overset{b}{c}_{ijkl}\frac{\partial \delta u_k}{\partial x_l}\right) = \frac{\partial}{\partial x_j}\left(\delta c_{ijkl}\frac{\partial u_k^b}{\partial x_l}\right) \ . \tag{A4}$$

Equation A1 can be solved in the frequency domain in terms of the Green's function using the representation theorem:

$$u_n(\mathbf{x}_r,\omega) = \int\limits_{V(\mathbf{x}')} h_i(\mathbf{x}',\omega)\, G_{ni}(\mathbf{x}_r,\mathbf{x}',\omega)\, dV(\mathbf{x}') \ , \tag{A5}$$

where $h_i(\mathbf{x}',\omega)$ is the force density at $\mathbf{x}'$, $G_{ni}(\mathbf{x}_r,\mathbf{x}',\omega)$ is the Green's function for the source at $\mathbf{x}'$ and receiver at $\mathbf{x}_r$, and $V(\mathbf{x}')$ represents the volume that includes all sources. To solve equation A4 for the scattered field, we replace $h_i(\mathbf{x}',\omega)$ in equation A5

by the right-hand side (source term) of equation A4:

$$\delta u_n(\mathbf{x}_r,\omega) = \int\limits_{V(\mathbf{x}')} \frac{\partial}{\partial x'_j}\left(\delta c_{ijkl}\,\frac{\partial u^b_k}{\partial x'_l}\right) G_{ni}\,dV(\mathbf{x}')$$

$$= \int\limits_{V(\mathbf{x}')} \left[\frac{\partial}{\partial x'_j}\left(\delta c_{ijkl}\,\frac{\partial u^b_k}{\partial x'_l}\,G_{ni}\right) - \delta c_{ijkl}\frac{\partial u^b_k}{\partial x'_l}\,\frac{\partial G_{ni}}{\partial x'_j}\right] dV(\mathbf{x}')\,. \tag{A6}$$

Applying the divergence theorem to the first term of equation A6 yields:

$$\delta u_n(\mathbf{x}_r,\omega) = \int\limits_{S(\mathbf{x}')} \delta c_{ijkl}\,\frac{\partial u^b_k}{\partial x'_l}\,G_{ni}\,\nu_j\,dS(\mathbf{x}') - \int\limits_{V(\mathbf{x}')} \delta c_{ijkl}\,\frac{\partial u^b_k}{\partial x'_l}\,\frac{\partial G_{ni}}{\partial x'_j}\,dV(\mathbf{x}')\,, \tag{A7}$$

where $S(\mathbf{x}')$ is the surface of the volume $V(\mathbf{x}')$, and $\boldsymbol{\nu}$ is the normal to $S(\mathbf{x}')$ pointing outward. Expanding the volume $V(\mathbf{x}')$ to infinity and using the radiation boundary condition (equation A3) reduces equation A7 to

$$\delta u_n(\mathbf{x}_r,\omega) = -\int\limits_{V(\mathbf{x}')} \delta c_{ijkl}(\mathbf{x}')\,\frac{\partial u^b_k(\mathbf{x}',\omega)}{\partial x'_l}\,\frac{\partial G_{ni}(\mathbf{x}_r,\mathbf{x}',\omega)}{\partial x'_j}\,dV(\mathbf{x}')\,. \tag{A8}$$

Here, the wavefield $\mathbf{u}^b$ is computed in the background medium and is generated by the force at the source location $\mathbf{x}_s$. Hence, $\mathbf{u}^b$ can be expressed in terms of the force applied at $\mathbf{x}_s$ and the Green's function:

$$u^b_k(\mathbf{x}',\omega) = f_m(\mathbf{x}_s,\omega)\,G_{km}(\mathbf{x}',\mathbf{x}_s,\omega)\,. \tag{A9}$$

Substituting equation A9 into equation A7 and using reciprocity,

$$G_{km}(\mathbf{x}',\mathbf{x}_s,\omega) = G_{mk}(\mathbf{x}_s,\mathbf{x}',\omega)\,, \tag{A10}$$

we find:

$$\delta u_n(\mathbf{x}_r,\omega) = -\int\limits_{V(\mathbf{x}')} f_m(\mathbf{x}_s,\omega)\,\delta c_{ijkl}(\mathbf{x}')\,\frac{\partial G_{mk}(\mathbf{x}_s,\mathbf{x}',\omega)}{\partial x'_l}\,\frac{\partial G_{ni}(\mathbf{x}_r,\mathbf{x}',\omega)}{\partial x'_j}\,dV(\mathbf{x}')\,, \tag{A11}$$

Next, we replace the Green's functions in equation A11 by their asymptotic representation (Vavryčuk, 2007),

$$G_{mk} = g^s_m\,g^s_k\,\bar{G}^s\,, \tag{A12}$$

$$G_{ni} = g^r_n\,g^r_i\,\bar{G}^r\,, \tag{A13}$$

where the superscripts s and r denote the source and receiver wavefields, respectively, $\mathbf{g}$ is the unit polarization vector, and

$$\bar{G}^s = \frac{1}{4\pi\rho\,V^s_{gr}\,R^s\,\sqrt{|K|}}\exp\left[i\frac{\pi}{2}\sigma_0 + i\,\omega\,\frac{\mathbf{p}^s}{v^s}\cdot(\mathbf{x}^s-\mathbf{x}')\right]\,, \tag{A14}$$

$$\bar{G}^r = \frac{1}{4\pi\rho\,V^r_{gr}\,R^r\,\sqrt{|K|}}\exp\left[i\frac{\pi}{2}\sigma_0 + i\,\omega\,\frac{\mathbf{p}^r}{v^r}\cdot(\mathbf{x}^r-\mathbf{x}')\right]\,. \tag{A15}$$

Here, V_{gr} and R are the group velocity and distance along the ray, K is the Gaussian curvature of the slowness surface, σ_0 is a function of K (Vavryčuk, 2007), $\mathbf{p}$ is the unit slowness vector, and v is the phase velocity.

Under the WKBJ approximation (e.g., Aki and Richards, 2002), the spatial derivatives are evaluated only for the rapidly varying terms of the Greens's functions (i.e., the exponent in equations A14 and A15). Substituting equations A12−A15 into equation A11 yields the following expression for the perturbed wavefield:

$$\delta u_n(\mathbf{x}_r,\omega) = \int\limits_{V(\mathbf{x}')} f_m(\mathbf{x}_s,\omega)\,\mathcal{A}(\omega)\,p^s_l\,p^r_j\,g^s_k\,g^r_i\,\delta c_{ijkl}\,dV(\mathbf{x}')\,, \tag{A16}$$

where

$$\mathcal{A}(\omega) = g^s_m\,g^r_n\,\bar{G}^s\,\bar{G}^r\,\frac{\omega^2}{v^s\,v^r}\,. \tag{A17}$$

The radiation pattern Ω for a model parameterized in terms of the stiffnesses is obtained as the amplitude of the kernel in equation A16 (i.e., the coefficient multiplied with δc_{ijkl}):

$$\Omega = p_l^s \, p_j^r \, g_k^s \, g_i^r \, . \tag{A18}$$

Here, we parameterize the model in terms of the velocities V_{P0}, V_{S0}, $V_{\rm nmo}$, and $V_{\rm hor}$. The stiffness coefficients represent the following functions of the velocities (Tsvankin, 2012):

$$C_{11} = \rho \, V_{\rm hor}^2, \tag{A19}$$

$$C_{33} = \rho \, V_{P0}^2, \tag{A20}$$

$$C_{13} = \rho \sqrt{(V_{P0}^2 - V_{S0}^2)(V_{\rm nmo}^2 - V_{S0}^2)} - \rho \, V_{S0}^2, \tag{A21}$$

$$C_{55} = \rho \, V_{S0}^2. \tag{A22}$$

The perturbation in the velocities can be expressed in terms of the perturbations in the stiffness coefficients using the chain rule. Since the background medium is isotropic, the background velocities satisfy $V_{\rm nmo} = V_{\rm hor} = V_{P0}$, and the unit polarization vectors are parallel (P-waves) or perpendicular (SV-waves) to the corresponding group velocity vector. For the P-wavefield, the 2D radiation patterns in the vertical plane are:

$$\Omega^P(V_{P0}) = 2 \, \rho \, V_{P0} \left[2 \, (p_3^s)^2 \, (p_3^r)^2 + (p_3^s)^2 \, (p_1^r)^2 + (p_1^s)^2 \, (p_3^r)^2 \right] , \tag{A23}$$

$$\Omega^P(V_{S0}) = 8 \, \rho \, V_{S0} \left[2 p_1^s \, p_3^s \, p_1^r \, p_3^r - (p_3^s)^2 \, (p_1^r)^2 - (p_1^s)^2 \, (p_3^r)^2 \right] , \tag{A24}$$

$$\Omega^P(V_{\rm nmo}) = 2 \, \rho \, V_{P0} \, \left(p_3^s \right)^2 \left(p_1^r \right)^2 + \left(p_1^s \right)^2 \left(p_3^r \right)^2 \, , \tag{A25}$$

$$\Omega^P(V_{\rm hor}) = 4 \, \rho \, V_{P0} \, \left(p_1^s \right)^2 \left(p_1^r \right)^2 \, . \tag{A26}$$

The patterns for the S-wavefield have the form:

$$\Omega^S(V_{P0}) = 0 \, , \tag{A27}$$

$$\Omega^S(V_{S0}) = 4 \, \rho \, V_{S0} \left[\left(p_1^s \, p_1^r + p_3^s \, p_3^r \right)^2 - \left(p_1^s \, p_3^r - p_3^s \, p_1^r \right)^2 \right] , \tag{A28}$$

$$\Omega^S(V_{\rm nmo}) = -4 \, \rho \, V_{P0} \, p_1^s \, p_3^s \, p_1^r \, p_3^r \, , \tag{A29}$$

$$\Omega^S(V_{\rm hor}) = 4 \, \rho \, V_{P0} \, p_1^s \, p_3^s \, p_1^r \, p_3^r \, . \tag{A30}$$

In the case of transmitted waves, because the incident and scattered angles are the same, the components of the unit slowness and polarization vectors for P-waves satisfy:

$$p_s^1 = g_s^1 = - \sin\theta \, , \tag{A31}$$

$$p_s^3 = g_s^3 = \cos\theta \, , \tag{A32}$$

$$p_r^1 = g_r^1 = \sin\theta \, , \tag{A33}$$

$$p_r^3 = g_r^3 = - \cos\theta \, , \tag{A34}$$

where θ is the phase angle with the (vertical) symmetry axis. For S-waves, the corresponding expressions are:

$$p_s^1 = -g_s^3 = - \sin\theta \, , \tag{A35}$$

$$p_s^3 = g_s^1 \quad = \cos\theta \, , \tag{A36}$$

$$p_r^1 = g_r^3 \quad = \sin\theta \, , \tag{A37}$$

$$p_r^3 = -g_r^1 = - \cos\theta \, . \tag{A38}$$